

# OPTIMIZING POSTBUCKLING COMPOSITE PANELS FOR DAMAGE RESISTANCE

Andrea A. Faggiani\*, Brian G. Falzon\*

\*Department of Aeronautics, Imperial College London, London, SW7 2AZ, United Kingdom

**Keywords:** *optimization, buckling, postbuckling, debonding, damage resistance*

## Abstract

*The design of current composite primary aerostructures, such as fuselage or wing stiffened panels, tends to be conservative due to the susceptibility of the relatively weak skin-stiffener interface. This weakness is due to through-thickness stresses which are exacerbated by deformations due to buckling. This paper presents a finite-element-based optimization strategy, utilizing a global-local modelling approach, for postbuckling stiffened panels which takes into account damage mechanisms which may lead to delamination and subsequent failure of the panel due to stiffener debonding. A genetic algorithm was linked to a finite element package to automate the iterative procedure and maximize the damage resistance of the panel in postbuckling. For a given loading condition, the procedure optimized the panel's skin layup leading to a design displaying superior damage resistance compared to non-optimized designs.*

## 1 Introduction

As more and more primary structures, in aircraft and aerospace vehicles, utilise composite material, it is imperative to fully understand the behaviour of composite structures under high loading. An example of this is the need to fully understand the postbuckling behaviour of stiffened composite panels. For instance, lower fuselage panels are primarily subject to compressive loads and are also vulnerable to the possibility of in-service damage due to runway debris or maintenance accidents. Considerable research effort has been expended in experimentally testing such panels and observing their buckling and postbuckling behaviour, looking at their failure modes, and also at optimizing various aspects of the panels to meet specific performance targets.

Experimental testing of composite panels involves loading the panels, typically in uniaxial compression, and then observing their structural behaviour as they first buckle and then enter the postbuckling regime. A variety of such tests have been conducted and the experimental results reported for panels of various dimensions and with hat, blade, J, and I-shaped stiffeners [1-7]. Many of the experimental programmes address the failure modes of the panels. It is widely indicated that failure is related to the initiation and progression of debonding between the skin and the stiffener at regions corresponding to buckle node and anti-node lines, due to the nature and magnitude of the stresses developing in this region. At a node line, a stiffener flange acts as a step change in the bending stiffness of the panel resulting in interlaminar shear stresses at this location. In contrast, at an anti-node line, the flange is pulled away from the skin due to the moment being transferred between the stiffener web and the stiffener flange/panel skin [3].

Optimization of composite plates subject to a variety of constraints and loads, being optimized for parameters such as buckling load or minimum weight has received a lot of attention [8-12]. When optimization involves integer variables, such as ply orientations in composite layers, genetic algorithms (GAs) [13] have proven to be very efficient [14, 15]. New and improved genetic operators have also been studied to improve the convergence rate of GAs, hence reducing computational cost, using methods such as localized searches and memory [16-18].

Work relating to optimization of complete composite panels is rather limited. Existing work includes optimization to minimize weight for a variety of load cases subject to stress, bending, and torsion buckling constraints [19], as well as minimum weight design under constrained postbuckling strength [20].

A more novel approach was investigated where in order to optimize stiffened panels for use in the

postbuckling regime, neural networks were used to replace non-linear FE analyses to evaluate the panel's postbuckling response. These were then linked to a GA to run the optimizations themselves. The optimization looked to obtain the highest possible ratio between the maximum allowable load and the buckling load, or constrained the prebuckling stiffness and buckling load and minimized the panel's weight [21].

All of the discussed optimization procedures suffer from the same limitation; they do not account for failure mechanisms which may occur prior to overall buckling collapse or due to in-plane structural failure. Such mechanisms are principally associated with delamination, particularly at the skin-stiffener interface, leading to a rapid degradation of the structural integrity of the panel as was evidenced by the experimental tests. This is a highly non-linear process, and is hence not suited to the use of neural networks. The present work describes an FE based optimization routine for postbuckling stiffened panels which takes into account delamination. First an I-stiffened panel was modelled in the FE package ABAQUS, and a global-local modelling approach was used together with cohesive elements to look at the panel's postbuckling behaviour as well as delamination initiation and progression. Results were compared to previously conducted experimental tests. Subsequently, a GA was set up and directly linked to the finite element package in order to optimize the stacking sequence of the panel skin so as to improve its damage resistance in postbuckling whilst imposing constraints on prebuckling stiffness and buckling load.

The GA was able to find an optimized stacking sequence of the panel skin to minimize the skin-stiffener debonding at a specific load level subject to the specified constraints.

## 2 I-Stiffened Panel

### 2.1 Panel Features

The panel optimized in this paper is an I-stiffened panel which was originally manufactured by BAE Systems. The panel was 604 mm wide and 850 mm long, and was reinforced by four I-stiffeners, equally spaced at 177 mm between their respective centrelines.

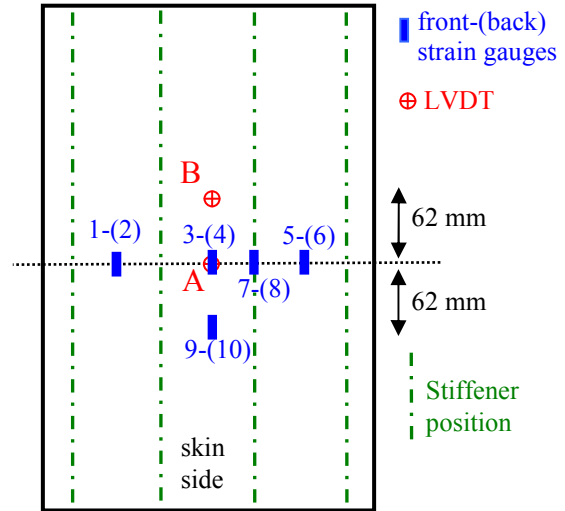


Fig. 1. Positioning of back-to-back strain gauges and LVDTs on I-stiffened panel

The stiffeners were secondary-bonded to the skin using FM-300 adhesive. The loaded edges at the ends of the panel were potted in a mixture of epoxy resin and fibreglass, before being machined flat and parallel, resulting in an effective span of 790 mm. The panel was compression tested under displacement control, with a crosshead displacement of 0.04mm/min. The Shadow Moiré Technique was used to qualitatively observe the out-of-plane displacements of the buckled skin, and back-to-back strain gauges and Linear Voltage Differential Transducers (LVDTs) were arranged at specific panel locations as shown in Fig. 1. The panel was made using T300/914C unidirectional prepreg, the nominal properties of which are shown in Table 1, while the skin and stiffener layup and dimensions are detailed in Fig. 2.

Table 1. Nominal material data

	T300/914C Unidirectional prepreg
$E_{11\text{tension}}$	135 GPa
$E_{11\text{compression}}$	120 GPa
$E_{22\text{tension}}$	9 GPa
$E_{22\text{compression}}$	9 GPa
$G_{12}$	4.9 GPa
$\nu_{12}$	0.28

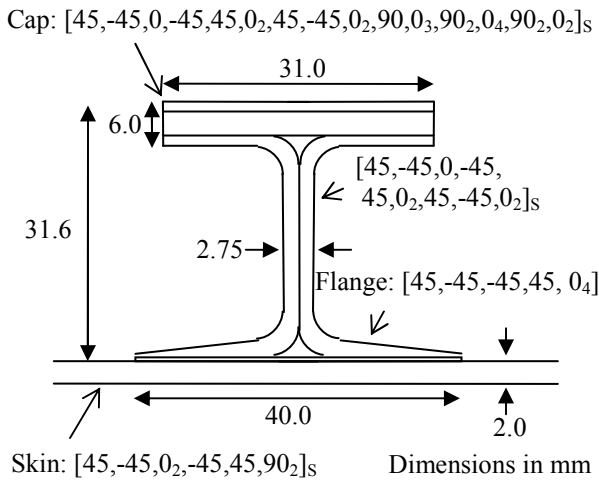


Fig. 2. I-stiffener cross section and layup

2.2 Experimental Results

2.2.1 Buckling and postbuckling

Buckling of the panel skin was seen to initiate at about 120 kN, with the first mode-shape being clearly visible at 160 kN as shown by the Moiré fringe patterns of Fig. 5 (a), which clearly show five half-waves in each of the skin-bays. Fig. 3 shows how back-to-back strain gauges 3 and 4, mounted on the panel centre in the mid bay and corresponding to the position of a buckle peak, displayed buckling at the critical load. A mode-switch occurred at 241 kN from five to six half-waves in each of the skin bays, illustrated in Fig. 5 (b). The location of the central node-line switched to an anti-node line, and as Fig. 3 shows, the longitudinal strains suddenly reduced. The mode jump was sudden and accompanied by an audible snap. Further cracking sounds took place at 308 kN, 361 kN, and 416 kN, while a loud crack was heard at 444 kN and three pops at 461 kN. At 473 kN another mode-shape change occurred in the left bay, and at 486 kN in the right bay. This was characterised by another sudden jump from six to seven half waves. The middle bay however stayed in the six half-wave configuration, but with the upper buckle being longer than the others, and possibly interacting with the upper buckles on the outer bays on either side as they appeared squeezed, as shown in Fig. 5 (c). More cracks were heard between 518 kN and 524 kN, preceding catastrophic failure at 525 kN.

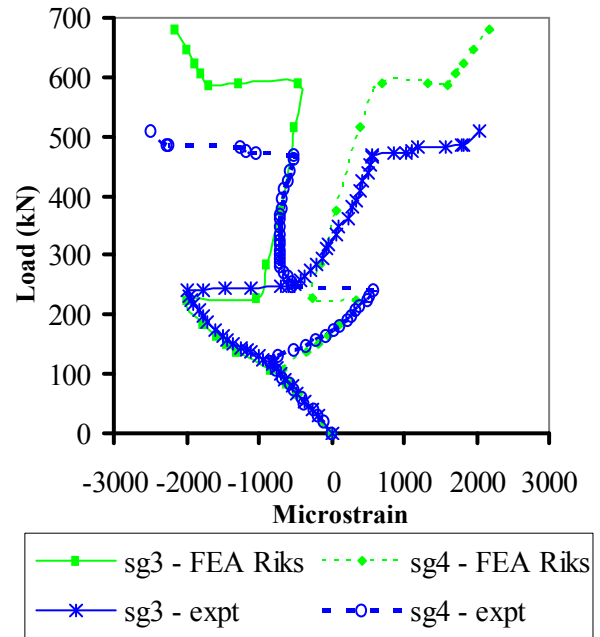


Fig. 3. Experimental and FEA Riks method back-to-back strain gauge results for sg3-sg4

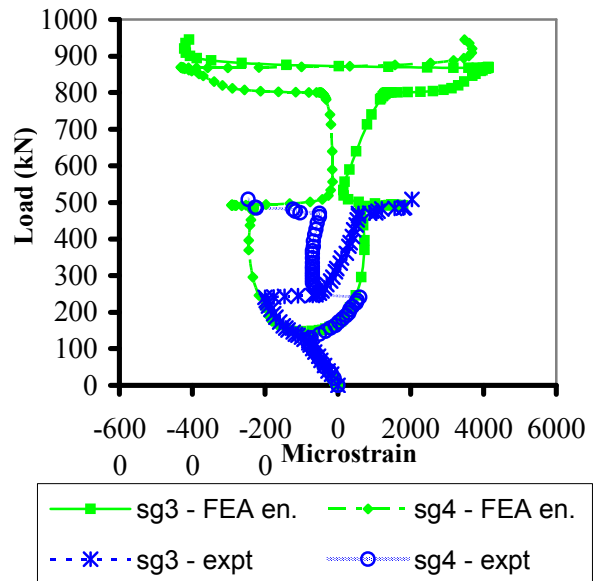


Fig. 4. Experimental and FEA energy dissipation scheme back-to-back strain gauge results for sg3-sg4

2.2.2 Panel Failure

After catastrophic failure at 525 kN, *in-situ* ultrasonic scans were conducted to try and understand the mechanisms of crack initiation and progression that led to failure. Ultrasonic scans at the anti-node lines, where transverse bending moment is at a maximum, showed potential delamination, but limitation of the ultrasound-scan procedure prevented accurate knowledge of failure initiation. Cerini [22] suggested a failure mechanism which initiated with the delamination of

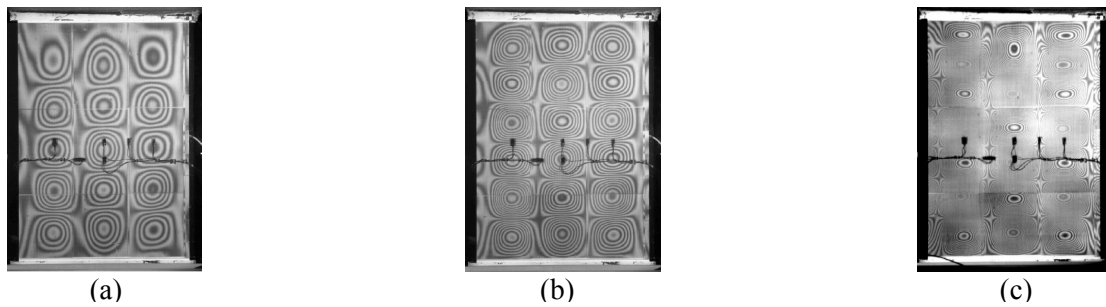


Fig. 5. Moiré fringe patterns for I-stiffened panel at (a) 160 kN, (b) 242 kN, (c) 487 kN loading

the skin-stiffener interface directly underneath one of the stiffener webs. This caused the skin to buckle outwards, peeling off the rest of the stiffener and subsequently a second stiffener. This resulted in the panel bending away from the stiffener side and collapsing globally. This failure mode agrees well with experimental work [3-7] which indicates that damage starts at the skin-stiffener interface of the panel at positions corresponding to buckle node and anti-node lines due to the stress concentrations in these regions.

### 2.3 FE Panel Model

The finite element package ABAQUS [23] was used to create a model of the experimental panel. Appropriate boundary conditions, reflecting the experimental conditions were applied to the model, which was meshed using 2760 4-node linear shell elements with six degrees-of-freedom at each node. Appropriate shell sections were defined to represent the layout of the panel. Linear buckling analyses were first conducted to find the buckling load and mode-shapes of the panel, and these were subsequently used to introduce geometric imperfections into the panel to eliminate bifurcation points. This allowed ABAQUS non-linear analysis algorithms to trace the full response of the panel past buckling and into the postbuckling regime. A linear superposition of the first three buckling modes was used to impose an out-of-plane displacement corresponding to 5% of the skin thickness, and both the modified Riks algorithm and energy dissipation schemes available in ABAQUS were utilized to trace the panel's response [23, 24].

### 2.4 FE Analysis Results

ABAQUS linear analyses predicted the I-stiffened panel to buckle at a load of 126.5 kN, in good agreement with the experimental buckling load of 120 kN. A five half-wave configuration was then predicted by the non-linear solver, in agreement with the experimentally observed initial buckle shape, as seen when comparing Fig. 5 (a) and Fig. 6 (a).

Good correlation (Fig. 3) was obtained between the strains at the panel centre as predicted by the ABAQUS modified Riks algorithm and those obtained experimentally as the panel entered its postbuckling regime. The FE analyses utilizing the modified Riks algorithm captured the jump from five to six half-waves, shown in Fig. 6 (b), but at a load of around 225 kN, lower than that observed experimentally. The further mode-jump to seven half-waves was predicted by ABAQUS at a loading past the actual experimental collapse load of the panel, as illustrated in Fig. 6 (c). At such high loading, micro-cracking may have occurred which is not captured by the FE model. The energy dissipation scheme in ABAQUS, introducing pseudo-damping forces to control instabilities, could only capture the behaviour of the panel qualitatively in its deep postbuckling regime. Fig. 4 shows the strains at the panel centre when using the energy dissipation scheme. The mode shapes are the same as those using the modified Riks method and shown in Fig. 6, but it is evident how the mode-jumps from five to six and from six to seven half-waves are predicted to occur at substantially higher loads than in the experiment.

Static path-following FE methods in ABAQUS showed that good quantitative agreement in the results was obtained for buckling and the initial postbuckling regime of the panel. Deeper in the postbuckling regime, only qualitative aspects of the panel's behaviour could be predicted. To improve this, and obtain a more complete and accurate prediction to the panel's behaviour, more efficient methods which combine static and dynamic solutions may be implemented [22, 25, 26].

## 3 Skin-stiffener Submodel

### 3.1 Submodel Features

The experimental results indicated that failure of the panel initiated due to debonding of the skin-stiffener interface. Because the FE model was

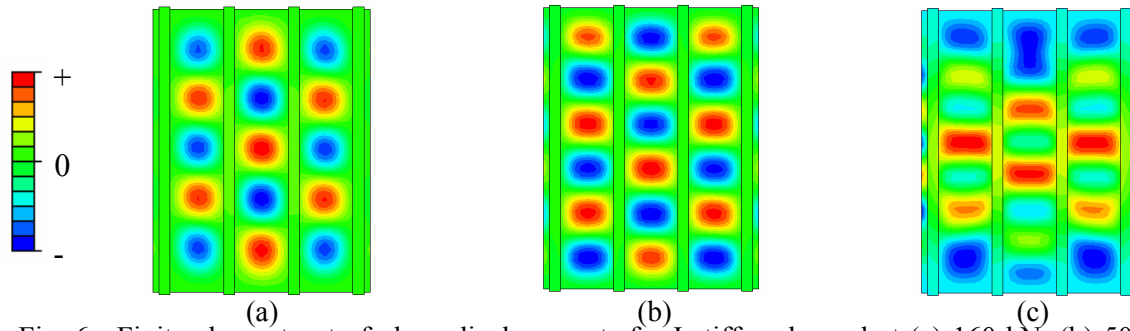


Fig. 6. Finite element out-of-plane displacements for I-stiffened panel at (a) 160 kN, (b) 500 kN, (c) 870 kN loading

composed entirely of shell elements with no failure modelling capability, it was unable to capture the rapid structural degradation. To model the delamination at the skin stiffener interface, a local model was created, corresponding to a section of the I-stiffened panel, shown in Fig. 7, chosen so as to analyze critical regions corresponding to node and anti-node lines. The local model was driven directly by the global model analyzed using the energy dissipation scheme, as the modified Riks algorithm is not supported in ABAQUS for submodelling purposes. The local model had a length of 197.5 mm and a width of 108.5 mm, with the stiffener containing 1344 8-node linear brick elements and 84 6-node triangular elements, and the skin 924 8-node linear brick elements. The use of brick elements allowed the possibility of capturing detailed geometric features such as ply drops in the flange region, as shown in Fig. 7. 336 8-node cohesive elements were introduced at the skin-stiffener interface to model the initiation and progression of delamination.

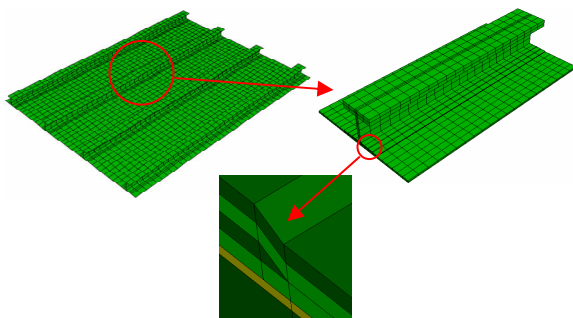


Fig. 7. Global and local models with associated ply drop detail in local model

### 3.2 ABAQUS Cohesive Elements

Interfacial decohesion elements, also known as interface elements, use failure criteria combining aspects from strength-based analysis, to predict the onset of softening, and fracture mechanics to predict

the propagation of delamination. The traction-separation model in ABAQUS is based on damage mechanics principles and involves an initial linear elastic behaviour followed by initiation and evolution of damage [27]. This approach also allows the combination of more than one damage mechanism to act at the same time on the cohesive interface. A quadratic nominal stress criterion was used for mixed mode damage initiation, and a Benzeggagh-Kenane (BK) [23] fracture energy based criterion for damage evolution under mixed mode conditions. ABAQUS assigns a damage level 0 in a cohesive element when no damage has initiated. A level of 1 indicates complete stiffness degradation and hence debonding. The adhesive used in the experimental I-stiffened panel to secondary bond the stiffener to the skin was FM-300, and appropriate values, obtained experimentally, were used to describe the traction-separation law. These are shown in Table 2.

Table 2. Skin-stiffener interface secondary bond properties.

	FM-300 Adhesive
film thickness	0.13 mm
$\sigma_{0I}$	61.0 MPa
$\sigma_{0II} / \sigma_{0III}$	49.8 MPa
$G_{IC}$	532 J/m <sup>2</sup>
$G_{IIIC} / G_{IIIC}$	2358 J/m <sup>2</sup>

### 3.3 Local Model FE Results

The local model containing the cohesive elements allowed for the level of debonding at the skin-stiffener interface to be investigated as the panel progressed through its postbuckling regime. Fig. 8 shows the local model in its deformed configuration (deformation scale factor 3). The stiffener is removed so as to show the level of degradation predicted by ABAQUS at the skin-

stiffener interface. At a load of 160 kN, shown in Fig 8 (a), the panel had buckled into its five half-wave configuration and there was very little degradation at the skin-stiffener interface. As the buckle crests grew, some degradation started occurring directly below the stiffener web at a location corresponding to an anti-node line as visible in Fig 8 (b). This agreed with experimental results which indicated that at an anti-node line the moment transfer between the stiffener web and the stiffener flange/panel skin acted to pull the flange away from the panel. At a loading of 500 kN, the panel had already jumped to a six half-wave configuration. This shifted the location of the node and anti-node lines on the local model as is evident in Fig 8 (c), resulting in the debonding spreading to the new anti-node locations. For very high loads, the panel had jumped to a seven half-wave configuration and the interface was almost completely debonded as can be seen in Fig. 8 (d).

#### 4 I-stiffened Panel Optimization

##### 4.1 Formulation of Optimization Problem

An optimization was formulated for the I-stiffened panel so as to find a revised stacking sequence for the panel skin. The objective of the optimization was to increase damage resistance of the panel in postbuckling. The objective function was defined as the sum of the damage variable in all the cohesive elements at the skin-stiffener interface, and hence this sum was to be minimized. A maximum end-displacement of 2.8 mm was chosen as this is past the buckling load of the panel and in its postbuckling regime. Constraints were set on the prebuckling stiffness and buckling load of the panel,

limiting them to no more than a 10% reduction.

First a linear buckling analysis was run on the global model to find the mode shapes which were required to be injected as an imperfection for the non-linear analysis of the global model. With the imperfection, the non-linear global analysis could be run, and its solution used to drive the local model quasi-static analysis to model the skin-stiffener debonding. The skin contained eight plies (symmetric) which were allowed to vary in the optimization process. These plies were limited to orientations of  $0^\circ$ ,  $45^\circ$ ,  $-45^\circ$ , and  $90^\circ$ , commonly used in industry. This implied a search space of 65,536 different layup possibilities. The optimization itself was conducted using a GA which linked directly to ABAQUS for the function evaluations. A GA was chosen because of the discrete nature of the problem.

#### 4.2 Genetic Algorithm

##### 4.2.1 Initial Population

The GA implemented for the panel optimization worked with a fixed size population. Each member of the population corresponded to a chromosome string representing a specific panel layup. Each string was then entered into the population matrix as an individual row entry. The initial population was created randomly, with every entry being an integer in the range 1-4, each number corresponding to one of the ply orientations.

##### 4.2.2 Constraints, Fitness and Selection

Once the population matrix was created, each individual was decoded into its actual layup. The ABAQUS global and local models were then

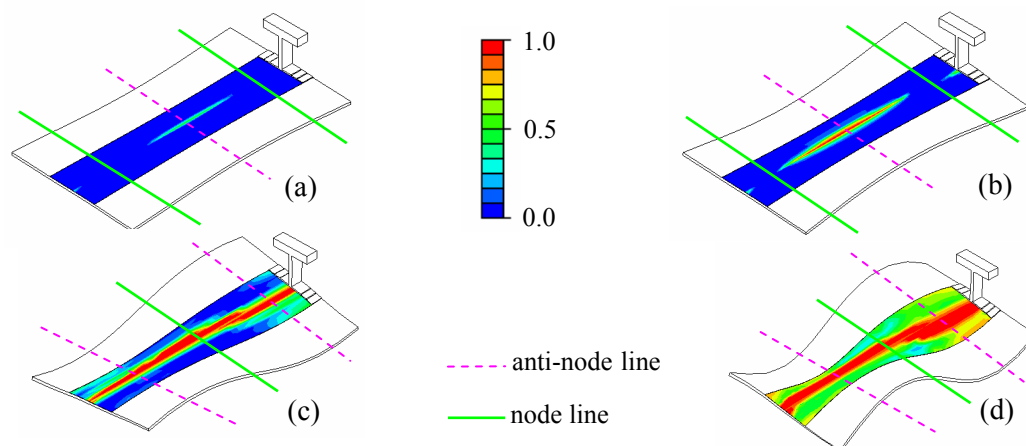


Fig. 8. Local model deformed shape and associated cohesive interface damage at (a) 160 kN, (b) 250 kN, (c) 500 kN, (d) 870 kN loading

updated to reflect the changes in the skin layup. Linear buckling analyses and non-linear analyses were run on the global model, followed by the local debonding analysis to calculate the objective function corresponding to the total damage at the skin-stiffener interface. The GA then assigned a fitness value to each individual based on the objective function. Rank-based fitness with a selective pressure of two was used, so that the individual with the lowest objective function and hence damage had a fitness of two, that with the highest objective function a fitness of zero, and all other individuals linearly assigned values in between.

Just prior to fitness assignment, the constraints on buckling load and prebuckling stiffness were imposed. For each individual found to violate one or more of the constraints, hence having a buckling load and/or prebuckling stiffness reduction of 10% or more compared to the non-optimized panel, a “penalty” quantity was added to the objective function, hence “virtually” increasing its damage and reducing its fitness.

Following fitness assignment, stochastic universal sampling was used for selection. Each individual was mapped to a segment of a line representing the entire population, with each segment’s length proportional to that individual’s fitness. Equidistant pointers were then created for the number of individuals to be selected for breeding, and the pointers’ position dictated which individuals were chosen by the GA.

4.2.3 Crossover and Mutation

Breeding of the selected individuals was done via two-point crossover, where two random cut-off points were chosen in each individual’s chromosome string and then exchanging genetic information to generate the offspring. For example, the two parents below would result in the indicated offspring:

Parent 1: 3 3 / 2 1 4 / 2 1 2  
 Parent 2: 4 1 / 3 2 3 / 1 1 4  
 Offspring 1: 3 3 / 3 2 3 / 2 1 2  
 Offspring 2: 4 1 / 2 1 4 / 1 1 4

Mutation was applied after crossover, so as to prevent the potential loss of favourable genetic traits and also to allow the crossover operator to remain effective in the later stages of the GA’s search. Mutation changed a random bit in each individual’s string with a very small probability, set to 1/N, where N=8, or the length of each individual’s chromosome string.

4.2.4 Reinsertion, Memory, and Termination

Once all the selected individuals underwent crossover and mutation to create the offspring, these were evaluated by calling up ABAQUS for the objective function evaluations. To re-insert the offspring into the population, a fitness based reinsertion method was used where the least fit members were replaced by the newly created offspring, keeping the population size constant.

A memory capability was added to the GA where the objective function of each individual was stored. This meant that prior to evaluating an individual, the GA would first scan its “memory” to see if that individual had been previously evaluated. If so, then the same objective function was used. This reduced computational cost considerably, since in the later stages of the genetic search, when the GA is converging, more and more individuals of the population have the same genetic string and hence objective function.

The GA was instructed to stop when a set number of successive individuals showed the same layup, meaning that an optimum had been found. A maximum number of 20 generations was set.

5 Optimization Results

5.1 Optimum Skin Layup and GA Convergence

The GA to find an optimized skin layup to minimize the damage in the panel was seen to converge after 14 generations. Fig. 9 shows the average objective function (the total interface damage in the cohesive elements) in an individual of the population in each generation as the genetic search progressed.

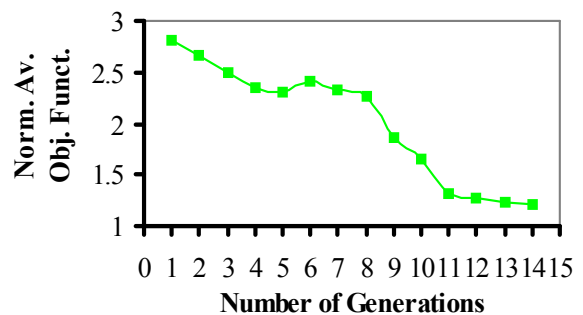


Fig. 9. Reduction of average normalized objective function with increasing GA generations

The objective function values are normalised with respect to the optimum found. As expected, the initial random population contained many individuals very far from the optimum, and hence

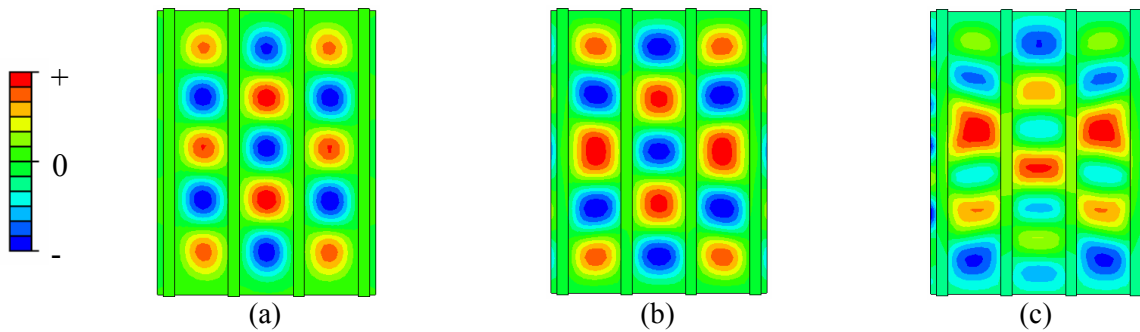


Fig. 10. Finite element out-of-plane displacements for optimized I-stiffened panel at (a) 160 kN, (b) 500 kN, (c) 870 kN loading

the average objective function was very high. As the GA was left to evolve, the average objective function dropped further and further until the optimum skin layup was found. The average normalised objective function once convergence has occurred is not quite as low as 1.0 as some individuals which have damage values higher than the optimum still remain in the population.

Table 3. Results comparing optimized and non-optimized panel skin configurations

	Non-optimized	Optimized	% Diff.
Skin Layup	[45,-45,0 <sub>2</sub> , -45,45,90 <sub>2</sub> ] <sub>s</sub>	[0,-45,45 <sub>2</sub> ,0,90, -45,90] <sub>s</sub>	
Buckling Load (kN)	126.5	122.2	-3.4%
Prebuckling Stiffness (kN/mm)	191.7	190.9	-0.4%
Postbuckling Stiffness (kN/mm)	155.6	155.1	-0.3%
Cohesive element Damage @ 2.8 mm	57.9	57.05	-1.5%

The optimum skin layup for the panel was found to be  $[0,-45,45_2,0,90,-45,90]_s$ . Table 3 compares the optimized configuration results to the non-optimized panel. The linear buckling analyses predicted a buckling load of 122.2 kN, 3.4% less than the value of 126.5 kN predicted for the non-optimized panel. The optimized panel's prebuckling stiffness was found to be 190.9 kN/mm, just 0.4% less than the non-optimized panel's 191.7 kN. These values showed how the constraints applied to the GA were effective in preserving the panel's stiffness and buckling load. The objective function of the optimized panel, the total damage in the cohesive elements for an applied end displacement of 2.8 mm, was found to be 57.05, compared to 57.9 for the non-optimized panel. This is a modest reduction of 1.5%, but it will be seen how further in the postbuckling regime the optimized panel displayed substantially less skin-stiffener debonding than the non-optimized one.

## 5.2 Optimized Panel Global Model Results

The postbuckling behaviour of the optimized panel was rather different to that of the non-optimized one. The global model results showed that in the optimized configuration the panel still buckled into five half waves, but the buckles were in the opposite direction as compared to the non-optimized case. This is clear when comparing Fig. 10 (a) with Fig. 6 (a). As the loading was increased, the revised skin layup meant that the optimized panel did not exhibit the mode jump to six half waves at the loading of 495 kN. Rather, as seen in Fig. 10 (b), the middle buckle crests in the right and left skin bays elongated, while the middle crest in the central bay became shorter. Thus, the panel retained the five half wave configuration further into its postbuckling regime. The side crests continued to grow, and the middle central crest became smaller until eventually a mode jump of the skin bays to six half-waves did occur at a loading of 830 kN, soon followed by the middle bay jumping to seven just before 870 kN as shown in Fig. 10 (c). At an even higher load the side bays followed suite and jumped to a seven half-wave configuration too.

## 5.3 Optimized Panel Local Model Results

To see how the change in postbuckling behaviour of the optimized panel relative to the non-optimized panel affected the skin-stiffener debonding, the local model results were investigated. Fig. 11 (a-b), when compared to the non optimized Fig. 8 (a-b), show very similar levels of debonding. What is clear though is how the panel is buckling in the opposite direction, but this does not influence the damage much. When the non-optimized panel mode jumps, in Fig 8 (c), the debonding at the skin-stiffener interface spreads due to the relocation of the anti-node lines. Since the optimized panel is not seen to mode jump at this

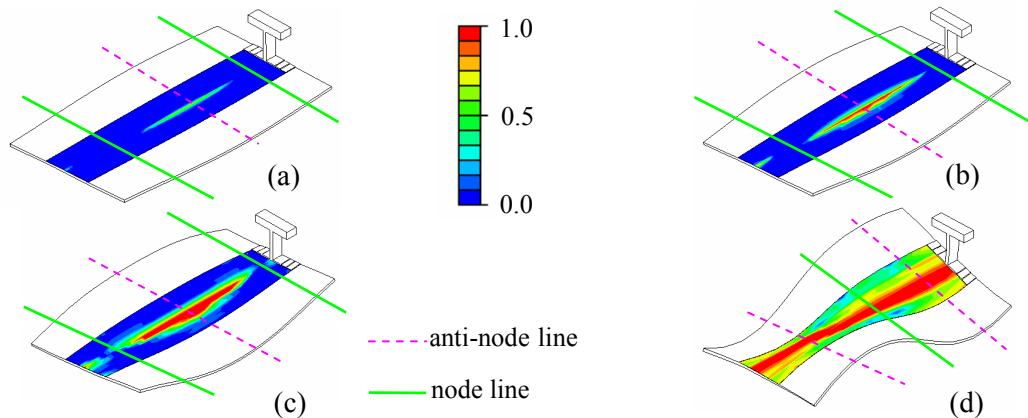


Fig. 11. Optimized panel local model deformed shape and associated cohesive interface damage at (a) 160 kN, (b) 250 kN, (c) 500 kN, (d) 870 kN loading

load, the damage remains localized and is hence reduced compared to the non-optimized panel. The buckle crests in the optimized panel elongated, hence the damage did somewhat spread, but did not extend across the whole length of the interface. When the optimized panel mode jumped at a higher load, then the node and anti-node lines changed locations and the interface became almost entirely debonded as seen in Fig. 11 (d).

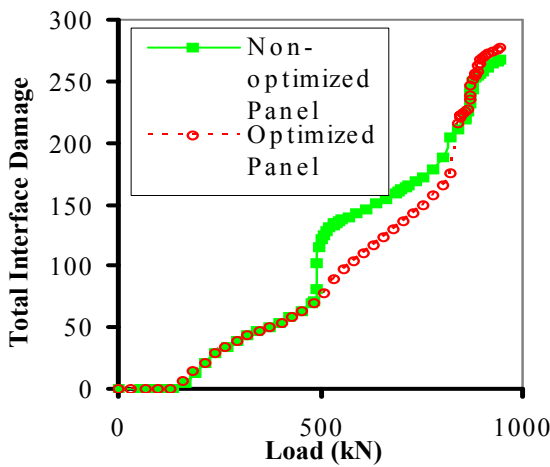


Fig. 12. Total damage progression with increasing end load for non-optimized and optimized panels

It is possible to trace the level of debonding as the loading on the non-optimised and optimized panels was increased. Fig. 12 shows a plot of the total interface damage, taken as the sum of the damage variable in the all the cohesive elements at the skin-stiffener local model interface, against the applied end load. It can be seen how the two panel configurations show very similar damage levels, until the non-optimized panel mode jumps at 495 kN at which point its total damage suddenly increases. The panel with the optimized skin layout remained in the five half-wave configuration for longer, and

hence such a damage increase was not visible until the mode jump at 830 kN. At such high loads the damages were again very similar as the skin-stiffener interface was almost completely debonded.

At the panel experimental collapse load of 525 kN, an investigation was conducted on the skin-stiffener interfaces of the non-optimized and optimized panels. It was seen that the total interface damage was reduced by 16.9% by optimizing the skin layout, and the number of cohesive elements displaying a degradation of more than 80% was reduced by 61.4%.

## 6 Conclusions

A global-local submodelling approach was used to accurately model the postbuckling behaviour of an I-stiffened panel. The global model traced the panel’s buckling and postbuckling response, while the local model was directly driven by the global solution and contained cohesive elements able to predict the skin-stiffener debonding caused by the stress concentrations arising at this interface.

The global and local models were directly linked to an optimization procedure which used a GA to optimize the skin layout of the panel so as to reduce the extent of skin-stiffener debonding in the postbuckling regime. Constraints were added so that the optimized design would have a buckling load and prebuckling stiffness reductions of no greater than 10% compared to the non-optimized design. The GA was able to find a revised skin layout which was effective in reducing the damage at the skin-stiffener interface. This occurred as a result of the change in the postbuckling behaviour of the panel, as a mode-jump to a different buckle configuration was delayed hence postponing the spreading of the debonding across the whole interface. At a load corresponding to the experimental collapse load, the

optimized panel was seen to have a total skin-stiffener interface damage of 16.9% less compared to the non-optimized configuration.

## References

- [1] Starnes Jr., J. H., Knight Jr., N. F. and Rouse, M. "Postbuckling behaviour of selected flat stiffened graphite-epoxy panels loaded in compression". *AIAA Journal*, Vol. 23, No. 8, pp 1236-1246, 1985.
- [2] Romeo, G. "Experimental investigation on advanced composite-stiffened structures under uniaxial compression and bending". *AIAA Journal*, Vol. 24, No. 11, pp 1823-1830, 1986.
- [3] Stevens, K. A., Ricci, R. and Davies, G. A. O. "Buckling and postbuckling of composite structures". *Composite Structures*, Vol. 26, No. 3, pp 189-199, 1995.
- [4] Falzon, B. G. and Stevens, G. P. "Buckling mode transition in hat-stiffened composite panels loaded in uniaxial compression". *Composite Structures*, Vol. 37, No. 2, pp 253-267, 1997.
- [5] Kong, C., Lee, I. C., Kim, C. G. and Hong, C. S. "Postbuckling and failure of stiffened composite panels under axial compression". *Composite Structures*, Vol. 42, No. 1, pp 13-21, 1998.
- [6] Falzon, B. G., Stevens, K. A. and Davies, G. A. O. "Postbuckling behaviour of a blade-stiffened composite panel loaded in uniaxial compression". *Composites Part A: Applied Science and Manufacturing*, Vol. 31, No. 5, pp 459-468, 2000.
- [7] Falzon, B. G. "The behaviour of damage tolerant hat-stiffened composite panels loaded in uniaxial compression". *Composites: Part A*, Vol. 32, No. 9, pp 1255-1262, 2001.
- [8] Chai, G. B., Ooi, K. T. and Khong, P. W. "Buckling strength optimization of laminated composite plates". *Composites & Structures*, Vol. 46, No. 1, pp 77-82, 1993.
- [9] Adali, S., Walker, M. and Verijenko, V. E. "Multi-objective optimization of laminated plates for maximum prebuckling, buckling and postbuckling strength using continuous and discrete ply angles". *Composite Structures*, Vol. 35, No. 1, pp 117-130, 1996.
- [10] Walker, M. "Optimal design of symmetric laminates with cutouts for maximum buckling load". *Computers & Structures*, Vol. 70, No. 3, pp 337-343, 1999.
- [11] Adali, S., Lene, F., Duvaut, G. and Chiaruttini, V. "Optimization of laminated composites subject to uncertain buckling loads". *Composite Structures*, Vol. 62, No. 3-4, pp 261-69, 2003.
- [12] Narita, Y. and Turvey, G. J. "Maximizing the buckling loads of symmetrically laminated composite rectangular plates using a layerwise optimization approach". *Proceedings of the Institution of Mechanical Engineers*, Vol. 218 Part C, No. 7, pp 681-691, 2004.
- [13] Goldberg, D. E. "Genetic algorithms in search, optimization, and machine learning". 1st edition, Addison-Wesley, London, 1989.
- [14] Le Riche, R. and Haftka, R. T. "Optimization of laminate stacking sequence for buckling load maximization by genetic algorithm". *AIAA Journal*, Vol. 31, No. 5, pp 951-970, 1993.
- [15] Le Riche, R. and Haftka, R. T. "Improved genetic algorithm for minimum thickness composite laminate design". *Composites Engineering*, Vol. 5, No. 2, pp 143-161, 1994.
- [16] Gantovnik, V. B., Gurdal, Z. and Watson, L. T. "A genetic algorithm with memory for optimal design of laminated sandwich composite panels". *Composite Structures*, Vol. 58, No. 4, pp 513-520, 2002.
- [17] Lin, C.-C. and Lee, Y.-J. "Stacking sequence optimization of laminated composite structures using genetic algorithm with local improvement". *Composite Structures*, Vol. 63, No. 3-4, pp 339-345, 2004.
- [18] Gantovnik, V. B., Anderson-Cook, C. M., Gurdal, Z. and Watson, L. T. "A genetic algorithm with memory for mixed discrete-continuous design optimization". *Computers & Structures*, Vol. 81, No. 20, pp 2003-2009, 2003.
- [19] Bushnell, D. "Optimization of composite, stiffened, imperfect panels under combined loads for service in the postbuckling regime". *Computer Methods in Applied Mechanics and Engineering*, Vol. 103, No. 1-2, pp 43-114, 1993.
- [20] Kang, J. and Chun-gon, K. "Minimum-weight design of compressively loaded composite plates and stiffened panels for postbuckling strength by genetic algorithm". *Proceedings of Proceeding of the 14th International Conference on Composite Materials (ICCM-14)*, San Diego, CA, pp 100, 2003.
- [21] Bisagni, C. and Lanzi, L. "Post-buckling optimization of composite stiffened panels using neural networks". *Composite Structures*, Vol. 58, No. 2, pp 237-247, 2002.
- [22] Cerini, M. "Investigation of secondary instabilities in postbuckling stiffened composite structures". PhD Thesis, Department of Aeronautics, Imperial College London, 2005.
- [23] ABAQUS. "ABAQUS 6.5 Documentation". 1st edition, Providence, RI, 2004.
- [24] Crisfield, M. A. "Non-linear finite element analysis of solids and structures". First Edition, John Wiley & Sons, Chichester, England, 1991.
- [25] Riks, E., Rankin, C. and Brogan, F. A. "On the solution of mode jumping phenomena in thin-walled shell structures". *Comput. Methods Appl. Mech. Engrg.*, Vol. 136, No. 1-2, pp 59-92, 1996.
- [26] Falzon, B. G. and Cerini, M. "An automated hybrid procedure for capturing mode-jumping in postbuckling composite stiffened structures". *Composite Structures*, Vol. 73, No. 2, pp 186-195, 2006.
- [27] Camanho, P. P. and Davila, C. G. "Mixed-mode decohesion finite elements for the simulation of delamination in composite materials". NASA-Technical Paper 211737, National Aeronautics and Space Agency, USA, 2002.